Journal of Energy Storage 37 (2021) 102412

Contents lists available at ScienceDirect

Journal of Energy Storage

journal homepage: www.elsevier.com/locate/est

Phytogenic generation of NiO nanoparticles as green-electrode material for high performance asymmetric supercapacitor applications

Sivagaami Sundari Gunasekaran [a], Arthi Gopalakrishnan [a], Raghu Subashchandrabose [b], Sushmee Badhulika [a,*]

[a] Department of Electrical Engineering, Indian Institute of Technology Hyderabad, Hyderabad 502285, India
[b] Center for Advance Energy and Alternative Fuels, Vels Institute of Science, Technology and Advanced Fuels, Chennai 600117, India

ARTICLE INFO

Keywords:
Green synthesis
Opuntia ficus-indica
NiO
Activated carbon
Asymmetric supercapacitor
Biomass

ABSTRACT

Herein, we report a simple, cost-effective, one-step green synthesis of nickel oxide nanoparticles (NiO—NPs) from *Opuntia ficus-indica* leaves extract for asymmetric supercapacitor application. The plant extract derived NiO—NPs exhibits an exceptional half-cell specific capacitance of 644 Fg^{-1} (~89.4 $mAhg^{-1}$) at 0.5 Ag^{-1}. The assembled asymmetric NiO—NPs|| activated carbon (AC) supercapacitor cell delivers high specific capacitance of ~280 Fg^{-1} (~38.8 $mAhg^{-1}$), excellent specific energy of 25 Wh kg^{-1}. In addition, the NiO—NPs|AC device works until 1.4 V with 0.1 M KOH as electrolyte delivering an excellent rate capability and high coulombic efficiency of 124% even after 10,000 cycles. Moreover, the biomass derived NiO NPs performs better than the other reported NiO based compounds, due to its presence of nickel-rich natural minerals. Through these findings, the use of plant leaves like *Opuntia ficus-indica* is hereby shown to be low-cost, environment-friendly alternative for preparing NiO- based composites for energy storage applications.

1. Introduction

Due to enormous consumption of fossil fuels and utilization of energy by the growing population, there is an urgent need in developing a sustainable energy storage device to meet the demand [1]. The design and fabrication of electrochemical energy storage systems with high flexibility, high energy and power densities dominate the majority of current rechargeable energy storage market [2]. In this regard, development of various high-performance energy storage devices such as fuel cells, batteries and supercapacitors (SCs) has gained enormous attention in recent years [3,4] Electrochemical supercapacitors (SCs) contribute to the high specific power, rapid charging-discharging, environmental friendliness, nontoxic nature and long-life cycle, which can meet the urgent need in the energy storage applications [1]. The energy storage performance of SCs mainly depends on various factors like electrochemical behavior of electrode material, electrolyte choice, and the operating potential window [2]. SCs have three classes namely, electric double layer capacitors (EDLC), pseudo-capacitors and battery SC hybrid (BSH) [5]. EDLC uses ion adsorption/desorption for the charging/discharging process (non-faradaic), whereas, pseudo-capacitors, uses oxidation–reduction reactions for charging and discharging (faradaic). BSH uses both faradaic and non-faradaic process charge storage mechanism. Due to the poor energy density of EDLC, pseudo-capacitors are gaining significant interest due to their highest theoretical specific capacitance and wide operating potential range [2]. Pseudocapacitors can provide much higher specific capacity and energy density than EDLCs, due to the large number ions participating in the redox reactions [6]. The carbon, carbon nanotubes are used as EDLC electrode materials, whereas meta oxides, hydroxides, sulphides are used as the pseudocapactior electrode material [3]. Carbon materials with high specific surface area, porosity and low cost were used as the electrode material for EDLC and their main drawbacks are the activation process, which involves lot of toxic chemicals [5]. There are variety of pseudocapacitance materials such as transition metal oxides or hydroxides or chalcogenides, metal sulfides, and conducting polymers [3]. Metal oxides offer attractive options as electrode material because of their high specific capacitance and low resistance, making it easy to create high energy and power SCs [6,7]. Therefore, in recent years development of various pseudocapacitive electrode materials has become a thrust research are to achieve much enhanced specific capacitance [8].

In particular, transition metal oxide NPs have attracted great interest

* Corresponding author.
E-mail address: sbadh@iith.ac.in (S. Badhulika).

https://doi.org/10.1016/j.est.2021.102412
Received 6 January 2021; Received in revised form 5 February 2021; Accepted 22 February 2021
Available online 20 March 2021

due to their significant physio-chemical and electrochemical properties such as enhanced charge storage property and efficient reversible redox reactions. Among various transition metal oxides like Fe_2O_3, SnO_2, and ZnO, the NiO material has shown promising supercapacitive performance due to its high electroactive sites with multiple oxidation states, abundancy, facile and low-cost synthesis route [3]. NiO has high electrochemical redox activity, cyclic reversibility, excellent durability and electrochemical stability and henceforth used as electrode material in supercapacitors [8]. Nanostructured NiO—NPs have been prepared using various methods like sol-gel [8], solvothermal [4], co-precipitation [9], thermal decomposition [10], polymer-matrix assisted synthesis [11], microwave [12], pulse laser ablation [13]. These techniques involve high energy, pressure, temperature, usage of toxic chemicals and longer reaction time strategies. Therefore, developing a simple and green synthesis routes for preparing NiO—NPs is of great significance in the area of affordable and sustainable synthesis approaches.

For example, Nwanya et.al., reported the synthesis of NiO—NPs using zea mays lea silk extract as a precursor through water-mediated synthesis. The synthesized nanoparticle delivered a specific capacitance of 54 Fg^{-1} at 5 mVs^{-1} [14]. Also, Reddy et.al, reported NiO—NPs composite from *Moringa oleifera* leaves by aqueous co-precipitation method. The prepared NiO—NPs delivered 350 Fg^{-1} at 0.5 mVs^{-1} [15]. From the above reported works, green synthesis of NPs has various advantages such as cost effectiveness, economic benefits, eco-friendly [16] than chemical or physical methods [17]. The plant extract serves as a fuel, capping agent and co-ordinates the capture the metal ion n the amylose helix in well-oriented sites. Moreover, there exist scant report on supercapacitor application using NiO NPs prepared via green synthesis route.

Herein, we report a novel one-step green synthesis of NiO—NPs from *Opuntia ficus-indica* plant-leaves extract as a new biomass source for high performance supercapacitor applications. *Opuntia ficus-indica* is from the polyphenol family which contains various flavonoids and phenolic acids. The chemical composition includes zinc 3.2 ± 0.3 mg/kg, manganese 1.9 ± 0.3 mg/kg, copper 2.1 ± 0.7 mg/kg and maximum potassium of 532.7 ± 11.7 mg/kg [18]. Since, the plant contains potassium as major composition, it can exhibit good electrochemical properties in the aqueous 6 M KOH electrolyte. The phenolic compounds, flavonoids, amino acids, proteins and lipids present in the extract acts a reducing and capping agent in the synthesis of NiO—NPs. In addition, due to the presence of nickel-rich natural minerals (garnierite), the formation of NiO—NPs is facile and efficient. The NiO NPs from the plant extract is obtained via ethanolic precipitation as a viable alternative to the chemical synthetic routes which releases large heat and toxic gasses. Moreover, the purity of the NiO nanoparticles obtained through the ethanolic precipitation is high compared to the water-induced precipitation [18]. The obtained NiO—NPs delivered high specific capacitance of 644 Fg^{-1} (~89.4 $mAhg^{-1}$) at 0.5 Ag^{-1}. The assembled ASC device employing activated carbon (AC) and the as-prepared NiO—NPs as the negative and positive electrode, respectively exhibited excellent energy of 25 Wh kg^{-1} at 40 W kg^{-1} with an outstanding cyclic stability. The ASC device has been fabricated with the NiO produced from this plant extract is the prime novelty of this work. NiO provides high pseudo-capacitance because of high-density faradaic actions. The NiO has been chosen for this work because of its low toxicity, low cost and higher abundance in biomass. Due to its multiple oxidation states, this NiO can be used in high-efficiency storage of electrochemical energy compared with carbon-based materials. NiO with AC with their synergic efficiency had contributed to the excellent specific capacitance, energy density and power density. To the best of our knowledge, this is the first report on NiO—NPs synthesized by green-protocol using new plant extract via ethanol precipitation for high-performance asymmetric supercapacitor applications.

2. Experimental section

2.1. Materials and reagents

The fresh leaves of *Opuntia ficus-indica*, ethanol, nickel nitrate hexahydrate [Ni $(NO_3)_2{\cdot}6H_2O$], de-ionized water, potassium hydroxide (KOH), dilute hydrochloric acid (HCl), isopropanol (99.5%), Nafion (60%) and Teflon solution were used without any modifications. All the reagents were of analytical grade.

2.2. Preparation of plant extract

The schematic representation of the synthesis of the nanoparticles has been represented in Fig. 1. The collected leaves of *Opuntia ficus-indica* were washed with running tap water and de-ionized water to remove the contaminants and air dried for about 2 weeks. The dried leaves were pulverized to dust particles. Further, 5 g of pulverized leaf dust mixed with 50 mL of ethanol solution were heated to 80 °C for 30 min. During the heating process, the phyto-chemicals are liberated which may contribute significantly to the electrochemical properties of the NPs. The phyto-chemicals like phenolic compounds, flavonoids, alkaloids, aspalathin, thiamine, riboflavin, niacin plays an important role as reducing and capping agent. The blend was cooled to room temperature and was filtered by Whatman filter paper (90 mm) and the obtained extract were stored in a cold condition (20 °C). It was then used for the further process.

2.3. Green synthesis of nickel-oxide nanoparticles

In brief, 0.1 M Ni $(NO_3)_2{\cdot}6H_2O$ were added drop wise to 20 mL of *Opuntia ficus-indica* leaf extract with constant stirring at ambient temperature. The formation of a black color mixture was observed which was then centrifuged at 10,000 rpm for 20 mins with de-ionized water in order to remove the unbound phytocompounds and impurities. The black color precipitate is the intermediate unstable $Ni(OH)_2$, which was annealed at 500 °C for 2 h under inert atmosphere to obtain NiO—NPs. The phenolic compounds with antioxidant potential in the leaf extract act as reducing agent while the other phytochemical moieties like amino acids, proteins and lipids act as capping agent to assist the nanoparticles synthesis.

2.4. Material characterization

The optimized NiO—NPs exhibit spherical-shaped agglomerated globules like morphology confirmed by field emission scanning electron spectroscopy (FE-SEM-Quattro S, Thermo Fischer Scientific, USA), while its oxidation states and electronic structure are confirmed by the x-ray photoelectron spectroscopy. X-ray diffractometer (XRD-Rigaku Smart Lab, Japan) with a copper source was used for studying the crystallinity of NiO—NPs. Raman spectrometer (RFS-100/S, Bruker, Germany) with laser excitation at 532 nm was employed for the recording of the Raman spectra of the NiO—NPs.

2.5. Electrochemical measurements

SP300 Biologic electrochemical workstation were used to evaluate all the electrochemical measurements using both two-electrode and three-electrode cell configuration. For three-electrode cell configuration, the electrode material was prepared by mixing 85% of NiO—NPs material with a homogenous suspension of 5% Nafion solution mixed with isopropanol and 10% acetylene black. It was then drop-casted onto the pre-cleaned glassy carbon electrode (GCE) (~0.1 mg) of 3 mm diameter and dried overnight in a vacuum at 80 °C.

CR2032 coin cells were used to fabricate the ASC with glass fibres as the separator and 0.1 M KOH as the electrolytic medium. The active material slurry was obtained by mixing NiO—NPs, carbon black, and

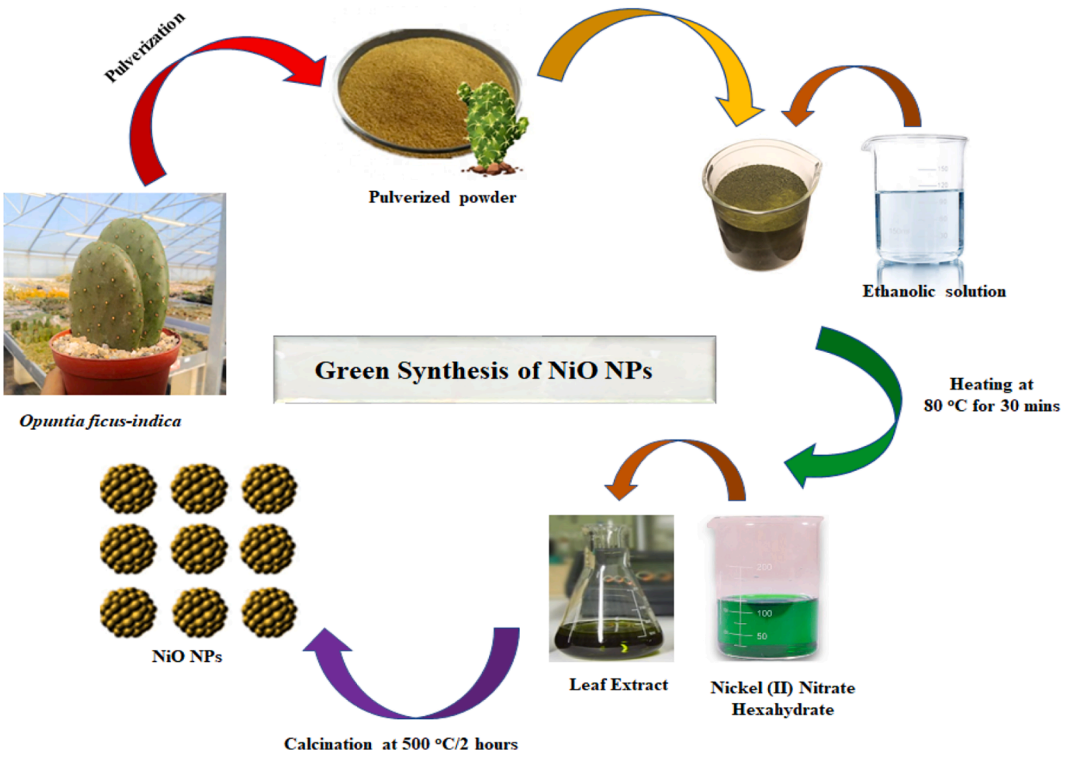

Fig. 1. Schematic representation of green synthesis of NiO—NPs.

Teflon solution (85:10:5)%w. The paste is made into a self-standing electrode film by drying in a vacuum at 120 °C for 2 h. Here, the NiO—NPs and AC are used as the cathode and anode, respectively.

Electrochemical performance of NiO—NPs was evaluated using cyclic voltammetry (CV), galvanostatic charge-discharge (GCD), electrochemical impedance spectroscopy (EIS) and cyclic stability study for the asymmetric supercapacitor applications. CV test was carried out within potential range of 0.3 V to 0.8 V at different scan rates 10–100 mVs^{-1} in 0.1 M KOH as the electrolyte. GCD were carried out for different current density 0.5,1,2,4,8,10,15 Ag^{-1}. The open-circuit voltage (OCV) was used for measuring the EIS spectrum with the frequency ranging from 0.01 Hz to 10 e^{-7} Hz.

The gravimetric specific capacitance (Fg^{-1}) of the electrode from CV profile was calculated using the below Eq. (1).

$$C = \frac{1000}{m \times v \times (Vc - Va)} \int_{Va}^{Vc} I(V)dV \quad (1)$$

m – electrode mass (mg), v-scan rate (mVs^{-1}), V_c and V_a -cathodic and anodic potential (V), I is the constant current (mA) and dV/dt is the discharge slope.

The specific capacity ($mAhg^{-1}$) of the electrode from CV profile was calculated using (2)

$$C = \frac{\int \mathrm{idV}}{2*3.6*m*V} \quad (2)$$

Where, ∫idV implies area under the CV curve, m is the mass of the electrode material (g), υ is the sweep rate.

From GCD, the specific capacitance of the NiO—NPs and the ASC cell was obtained using Eq. (2).

$$C_s = \frac{I\Delta t}{M\Delta V} \quad (3)$$

I-current (A), Δt -discharge time (s), M- total electrode mass (g), and ΔV-discharge potential (V).

From GCD, the specific capacity of the NiO—NPs and the assembled ASC device can be determined by (4).

$$C = \frac{I\Delta t}{3.6*M} \quad (4)$$

Where, I is the current density, Δt is the discharge time.

The specific energy ($Wh\ kg^{-1}$) of the ASC is calculated from Eq. (5).

$$E = \frac{1}{2*3.6} C_s V^2 \quad (5)$$

The specific power ($W\ kg^{-1}$) is calculated from the Eq. (6).

$$P = \frac{3600 \times E}{t} \quad (6)$$

3. Result and discussion

3.1. Elemental and morphological investigation of NiO-NPs

The surface morphology study of the as-synthesized NiO—NPs were studied using SEM images as given in Fig. 2(a, b). The results show randomly distributed smaller sized with homogeneous spherical shaped globule like particles, where some are in elongated form. The diameter of nanoparticles ranges from 20–34 nm. From 2(c) the EDAX spectrum of the prepared NiO—NPs reveals the presence of nickel and oxygen element without any other impurities [18]. The higher oxygen content is due to the large surface oxidation in addition to the obtained NiO sample.

3.2. Structural analysis of NiO-NPs

The structural information and crystallinity of prepared NiO—NPs were studied by XRD technique, which is represented in Fig. 3(a). The five characteristic peaks for NiO NPs at 2θ= 36.22, 42.77, 61.97, 72.02, and 75.97 ° corresponds to the Miller planes (111), (200), (220), (311), and (222), respectively. The peak at 2θ=29 represents the (110) plane.

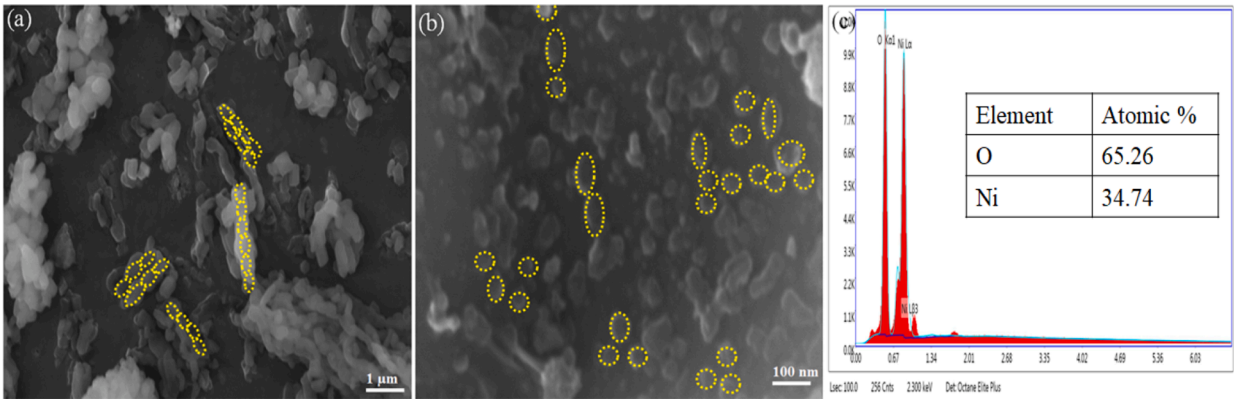

Fig. 2. FESEM image of NiO nanoparticles (a) at lower magnification (b) at higher magnification (c) EDAX spectrum.

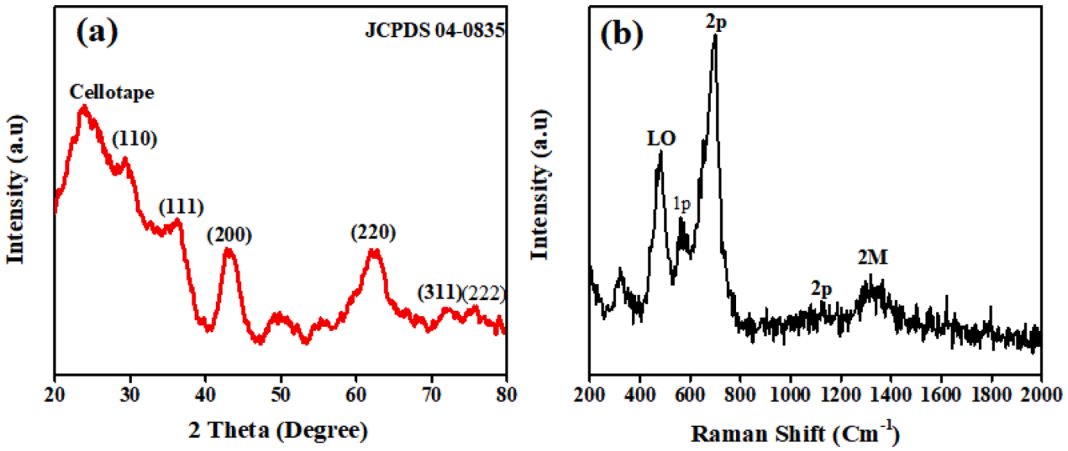

Fig. 3. (a) XRD pattern and (b) Raman spectrum of NiO NPs.

However, they are not properly aligned to produce a diffraction peak. As perpendicular to those planes does not bisect the incident and diffracted beams. Only the background is observed. Also, the peak at 2θ=23 arises due to the cellotape used for the XRD setup. These overall results represent the face-centered cubic (fcc) structure of NiO with JCPDS 04–0835 [19].

The Raman spectrum of NiO NPs is represented in Fig. 3(b). There are about 5 different prominent peaks at ~600 cm^{-1}, ~800 cm^{-1} - ~1200 cm^{-1} and ~1300 cm^{-1}, corresponding to 1P (one-phonon) TO and LO modes, 2P (two-phonon) 2TO modes, 2 M (two-magnon) scattering modes, respectively. The 1P bad which is the disorder-induced band has smaller intensity indicating the good-quality of the single-crystal of NiO NP with the presence of little defects due to the surface effects. The high intensity 2P band corresponds to the detectability for 100 nm crystallite size of the material at ambient temperature. The LO band, which is the first-order longitudinal optical property, can be related to the activation of the Raman vibration that causes a slight rhombohedral distortion in bulk NiO [20].

X-ray photoelectron spectroscopy (XPS) was studied to investigate the elemental valence state of the as-prepared NiO NPs. Fig. 4(a) which is the survey spectrum of the prepared NiO NPs, reveals the presence of nickel, carbon and oxygen without any impurities. Fig. 4(b) represents the high-resolution Ni 2p spectrum which displays a two-prominent main-peaks at ~855 eV and ~875 eV, corresponds the Ni $2p_{1/2}$ and Ni $2p_{3/2}$, respectively, which contributes to the redox reactions of +3 and +2 states of NiO in the electrochemical performance [21]. The peaks at ~863 eV and ~883 eV corresponds to the satellite peaks which are due change in coulombic potential. The C1s profile which is the reference profile is depicted in Fig. 4(c). According to the strong C—C/$C = C$ peak appearing at 284 eV, it is evident that the oxygen functionalities are sufficiently reduced by the thermal annealing treatment, which ensures good conductivity of the material. The deconvoluted O1s spectrum (Fig. 4(d)) has a peak at ~532 eV which is due to the oxygen functional group bonded with the nickel in the NiO, with $Ni^{3+}$with vacancy and deficiency, which can be attributed to the presence of more positive charge, that is helpful in capacitance enhancement [22].

3.3. Electrochemical performance in a three-electrode cell

To investigate the electrochemical performance of the individual NiO electrode material, CV, Galvanostatic-discharge techniques were employed in three-electrode cell configuration. Fig. 5(a) represents the CV curves of NiO NPs at increasing scan rates from 10 to 100 mVs^{-1}. Two-strong symmetrical anodic and cathodic peak are found at 0.52 V and 0.58 V which reveals the excellent reversible redox behavior of NiO—NPs [23]. The obtained redox peaks capacitance is mainly derived from surface faradiac reaction, contributing to the pseudo-capacitance [24]. The maximum specific capacitance of ~644 Fg^{-1} is obtained for the NiO—NPs at a scan rate of 10 mVs^{-1}. This value is higher than the previously reported results for NiO—NPs with different capacity [25]. Fig. 5(b) represents the capacitive and diffusion-controlled contribution to the charge storage of NiO—NPs. The EDLC represents to the capacitive contribution and the pseudo-capacitance represents the diffusion-controlled contribution. The capacitive and diffusion-controlled contribution can be evaluated using the equation [10],

$$i(V) = K_1 v + K_2 v^{1/2} \quad (7)$$

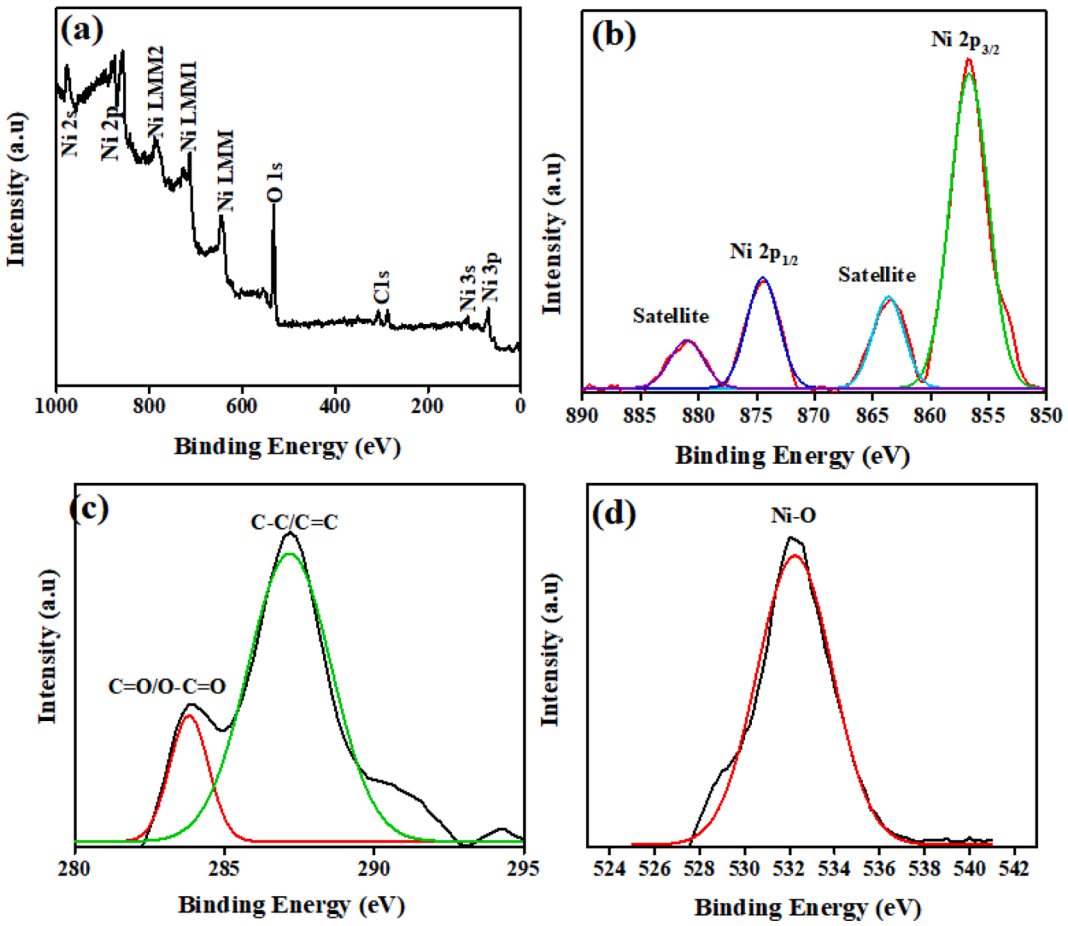

Fig. 4. XPS spectra of NiO NPs: (a) Survey Spectrum; high-resolution spectrum of (b) Ni 2p and (c) C 1 s (d) O 1 s.

where, i is the obtained current, V is the potential, υ is the operating sweep rates. The values of K_1 and K_2 is determined by employing CV currents at different scan rates. K_1 corresponds to the fraction of current from the surface capacitance (EDLC), whereas K_2 corresponds to the fraction current from the diffusion-controlled process (pseudo-capacitance). The figure represented, shows the typical voltage profile for the capacitive current (black) in comparison with the total current at a scan rate of 20 mVs^{-1}. It can be detected that the capacitive effect in prepared NiO is about ~5–10%, indicating a diffusion-controlled process of about ~90%, respectively. The percentage of EDLC is very smaller for the prepared NiO, which is due to the typical battery characteristic of material, which performance charge-storage through faradaic adsorption/desorption mechanism [26]. The capacitive process is enlarged in the insert for the clarification.

Further, to evaluate the electrochemical performance of NiO—NPs the GCD study was carried out (Fig. 5(c)). Different current densities (0.5 to 15 Ag^{-1}) were performed and is seen that lower the current given, the longer is the discharging time of the material, which is significant for the pseudo-capacitors [27,28]. The highest capacitance of NiO—NPs was calculated to be ~640 Fg^{-1} (~88.8 $mAhg^{-1}$) at 0.5 Ag^{-1}. This exceptional performance can be attributed to the presence functional groups like C, H, O, N-containing organic compounds in the leaf extract which will create more active sites and quick diffusion pathways. This enhanced capacitance can also be attributed to the surface area of the NiO—NPs material which is found to be ~275 m^2g^{-1}. Fig. 5(c) represents the comparison of specific capacitance of NiO—NPs at different current densities. It can be found that the specific capacitance is inversely proportional to the current density. The diffusion of electrolytic ions onto the active material happens at the lower current density. In contrast, the diffusion is limited at the higher current density [29]. The maximum capacitance of ~644 Fg^{-1} (~89.4 $mAhg^{-1}$) at 0.5 Ag^{-1}) is significantly higher than the previous reported NiO-based materials [30]. This is due to the phytochemicals which is present in the plant extract which acts as the capping agent and catalytic agent for the enhanced electrochemical performance. The plant extract induces carbon, oxygen and N-containing organic compounds into the synthesized nanoparticle. And this acquired carbon and oxygen-containing surface functional groups improves the conductivity and specific capacitance of the electrode material.

3.4. *Electrochemical performance of NiO NPs||AC*

To evaluate the performance of NiO NPs||AC ASC device, a two-electrode cell configuration was measured as represented in Fig. 6(a-c). Fig. 6(a) shows CV profile of the individual electrode activated carbon (AC) and the prepared NiO—NPs at 20 mVs^{-1}. The AC delivered rectangular shape CV curve without any redox peak which contributes to the EDLC behavior, whereas the NiO—NPs showed distorted redox peak contributing to the pseudo-capacitive behavior. For AC, the potential window of 0 V to −1 V were chosen. For the prepared NiO NPs, as the redox potential was found between 0.5 V-0.6 V, the potential window of 0.3 V to 0.8 V was opted. The potential of both AC and NiO—NPs in the assembled ASC device delivers the potential window of 0–1.4 V. Also, due to more active sites in the NiO—NPs, water-splitting takes place and paves way for the oxygen evolution reactions beyond 0.7 V. Fig. 6(b) represents the CV curve of the assembled ASC device at increasing potential window from 1 V to 1.4 V and hence the maximum voltage operated is optimized. As the voltage window is increased, the area under the CV curve is also increased, which can contribute to the

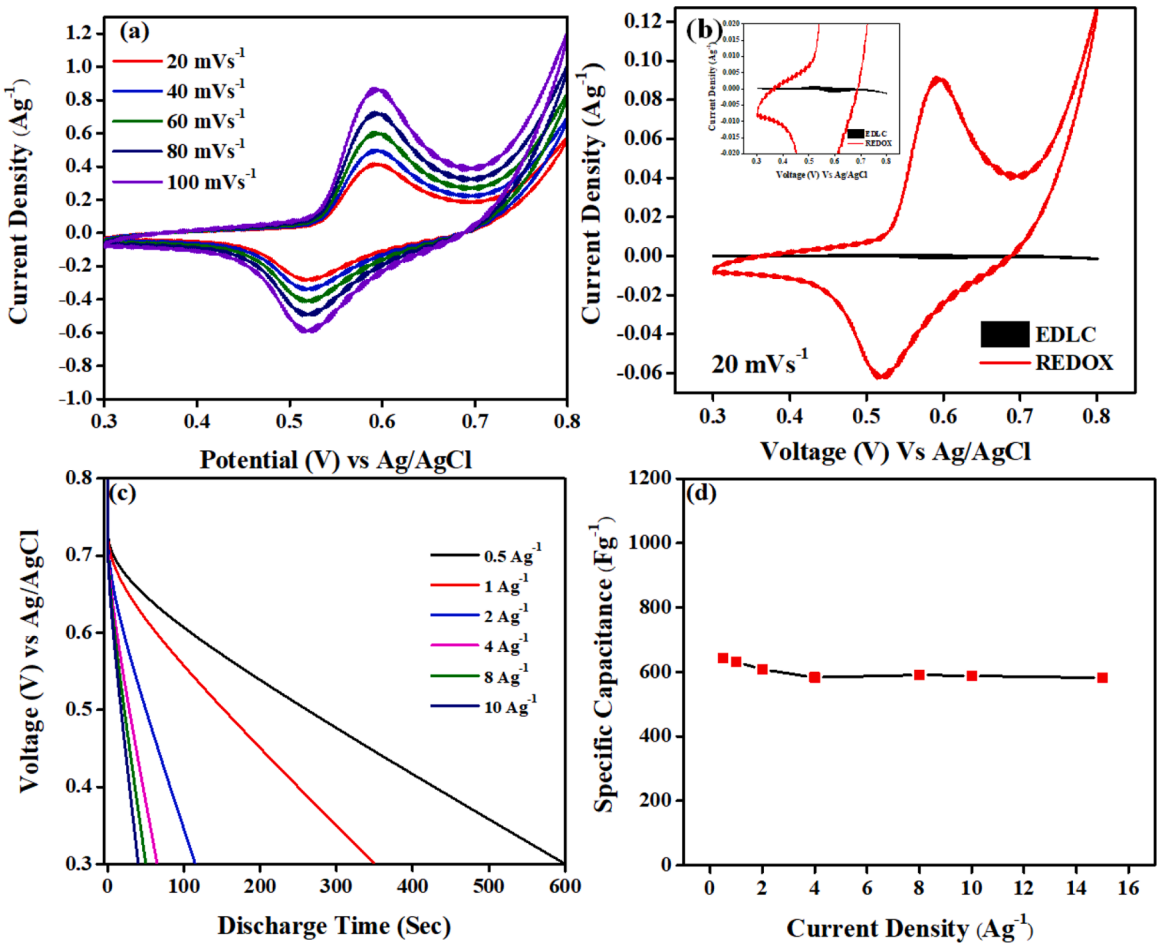

Fig. 5. (a) Cyclic voltammograms of prepared NiO NPs at different scan rates in 0.1 M KOH (b) CV curve of capacitive and diffused control process of the NiO—NPs at 20 mVs^{-1} insert: capacitive process enlarged (c) Galvanostatic-discharge curve of NiO—NPs at different current density (d) Specific capacitance of prepared NiO—NPs at different current density.

enhancement in the specific capacitance. Also, the redox peak is slightly shifted higher potential value. Fig. 6(c) represents the CV profile of ASC device at different scan rates 10–100 mVs^{-1}. From the result, it is clearly evident that, the current density and the operating sweep rate is directly proportional to each other. Fig. 6(d) represents the capacitive and diffusion-controlled contribution to the charge storage of the assembled ASC device. The capacitive and diffusion-controlled contribution is determined using the Eq. (7) and found to have ~10% of EDLC and ~90% of pseudocapacitance. This result confirms that the charge-storage in the assembled ASC device is predominately by the battery type electrode through faradaic redox reactions. The insert enlarges the EDLC contribution for the clarity.

Fig. 6(e) represents the GCD curve at increasing voltage. As the voltage is increases, the discharge also increases, which can be suitable for the high-performance supercapacitor applications. Fig. 6(f) represents the GCD profile of ASC device at increasing current densities from 0.5 Ag^{-1} to 10 Ag^{-1}. The curves obtained are irregular and non-symmetrical not similar to the EDLC [31,32]. Faradaic reaction involved in the reaction is given below.

$$NiO + (OH) \leftrightarrow NiOOH + e^{-}$$

The maximum capacitance from CV and GCD technique were calculated to be ~276 Fg^{-1} at 10 mVs^{-1} and 280 Fg^{-1} (~38.8 $mAhg^{-1}$) at 0.5 Ag^{-1}, respectively which is due to the short path for the ionic transport and good electrical conductivity of NiO NPs||AC materials. Also, the functional groups such as C, H, O, N-related functional groups from the plant extract change the electronic structure, morphology of the material and will create more active sites and quick diffusion pathways. Thus, the plant extract significantly improves the super-capacitive properties of the as-prepared NiO NPs [33].

3.5. *Stability of NiO NPs||AC ASC*

The diffusion kinetics of electrolytes ions within the active sites of the electrodes are determined by the EIS techniques [34]. Fig. 7(a) shows the Nyquist plots for the NiO—NPs|AC ASC device before and after cycling analyzed by EIS. The diffusion of ions in the electrode material can be contributed to a small-depressed semi-circle which is found in the high-frequency region and a vertical line is found in the low-frequency region [35]. From the EIS spectrum, it is seen that the low-frequency straight line is almost vertical and thus contributing to the improved capacitive behavior of the electrode material [36]. The series resistance is found to be 0.23 Ω, indicating its better charge-discharge rates enhancing the specific capacitance and specific energy of the ASC device [37]. The series resistance after the cycling is found to be ~13.4 Ω. The resistance value has been increased after the cycling process due to the formation of an SEI layer (Solid electrolyte interfase) layer between the electrode and the electrolyte. The Ragone's plot which is the plot between the specific energy and specific power of the ASC device is shown in Fig. 7(b). The plot showed the linear performance, which attributed to the significant supercapacitor behavior. The maximum specific energy was found to be ~25 $Whkg^{-1}$ at 0.5 Ag^{-1} and the maximum specific power was found to be ~40 Wkg^{-1} at 15 Ag^{-1}. The long-term stability of the cycle is typically needed for the

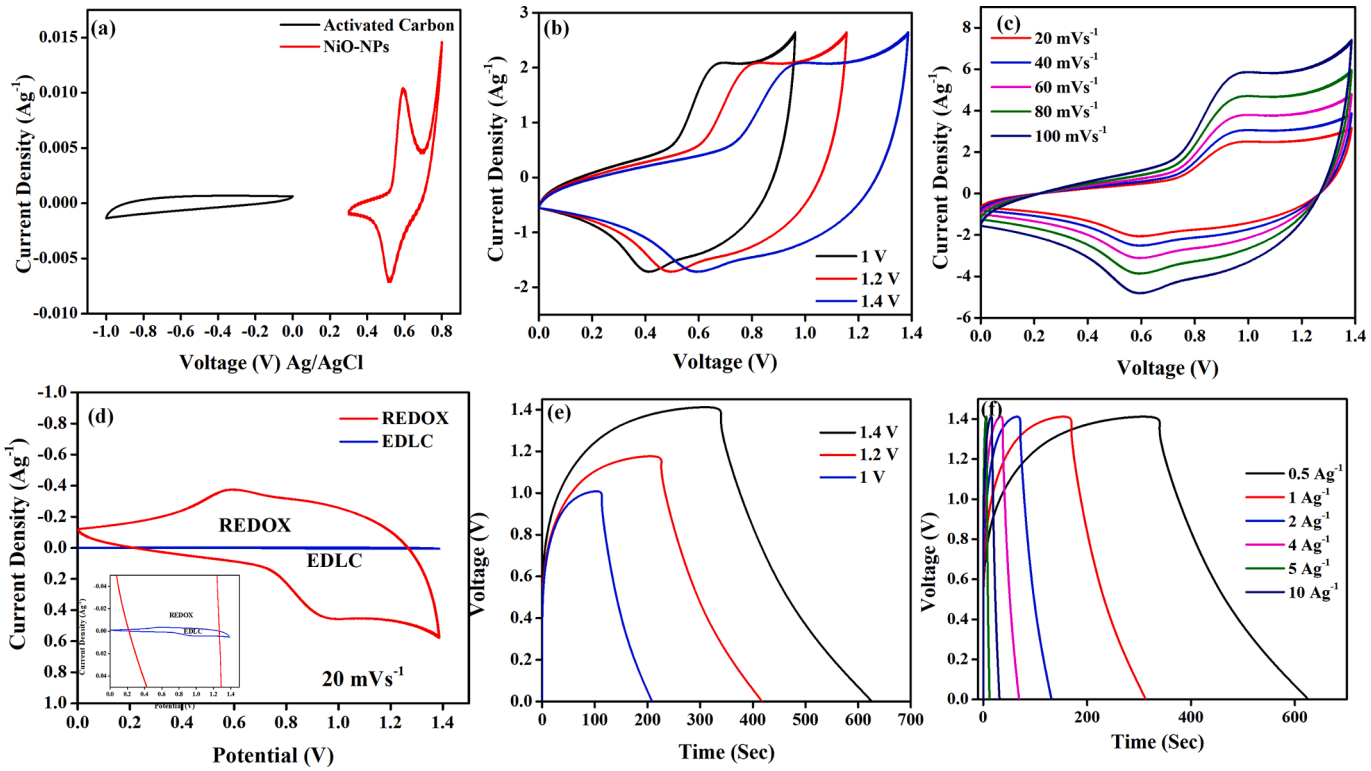

Fig. 6. (a) comparison of CV profile of AC with prepared NiO—NPs (b) CV at different voltage window (c) CV at different scan rates (d) Capacitive and diffusion-controlled contribution to the charge storage. Insert: EDLC contribution (e) GCD at different voltage (f) GCD at increasing current density of the assembled ASC device.

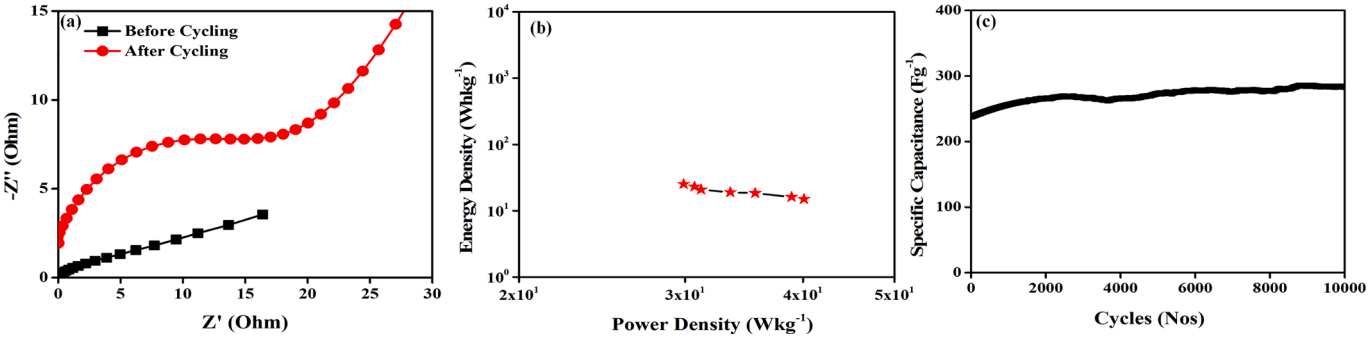

Fig. 7. (a) EIS-Nyquist spectrum before and after cycling (b) Ragone's plot (c) Cyclic study of ASC device.

practical supercapacitor performance. The cyclic charge-discharge of the ASC device was studied at 1 Ag^{-1} over 10,000 cycles and the results are depicted in Fig. 7(c). The enhancement in the specific capacitance till 9000+ cycles is attributed to the activation process of the electrode material. Also, the accessibility of more pore sites within the active material after several constant GCD cycles contributes to the

Table 1
Comparison of half-cell specific capacitance of prepared NiO with recent NiO nanomaterials-based reports.

S. No	Material	Synthesis Techniques	Specific Capacitance (F g^{-1})	Cyclic Stability (No. of cycles)	References
1.	NiO Nanoparticle	Co-Precipitation from *E. cognate*	74	–	[38]
2.	NiO Nanoparticle	Homogeneous precipitation method	390	82.8% in 5000 cycles	[40]
3.	NiO Nanoflakes	Microwave assisted	401	–	[41]
4.	NiO Nanocrystals	Hydrothermal Process	390	–	[42]
5.	NiO Thin film	Chemical Deposition	167	–	[43]
6.	NiO Nanosheet	Hydrothermal	81.67	78.5% in 5000 cycles	[44]
7.	NiO Nanoarray	Electrochemical precipitation	277	–	[45]
8.	NiO Thin flim	Hydrothermal Method	270	93% in 500 cycles	[46]
9.	NiO Nanofiber	Electrospinning	336	87% in 200 cycles	[47]
10.	**NiO Nanoglobule**	**Ethanolic precipitation from *Opuntia ficus-indica* plant extract**	**644**	**96.5% in 10,000 cycles**	**This Work**

performance. The capacitance retention is calculated from the following equation,

$$Capacitance\ Retention\ (\%) = 100^{*}\frac{Final\ Capacitance}{Initial\ Capacitance}$$

The initial capacitance of ~ 273 Fg^{-1} of the ASC device was used to calculate the capacitance retention. After 1000 cycles, the ASC delivers 124% capacitance retention, due to the redox reactions during cycling performance indicating its excellent cyclic stability [38,39].

The performance of the NiO—NPs derived from *Opuntia ficus-indica* plant extract is compared with recently reported NiO—NPs synthesized using different methodologies, as shown in Table 1. Most of these materials are synthesized using multi-step process that use expensive and toxic reagents. In addition, techniques like microwave, chemical vapor deposition, hydrothermal along with requirement of higher temperature and pressure are used for the synthesis. Also, the ASC device from other NiO—NPs deliver narrow potential window (below 1.2 V). In this work, we report the synthesis of NiO—NPS by a green synthetic route which simplifies the synthesis approach and prevails over the above-mentioned limitations. To the best of our knowledge, this is the first report of ASC with green electrode, extending its potential window till 1.4 V.

4. Conclusion

In summary, NiO—NPs were successfully synthesized from *Opuntia ficus-indica* leaves extract as new biomass source by green biosynthesis technique, towards supercapacitor applications. The presence of phytochemicals present in the plant extract acts as a capping and catalytic agent for the formation of NiO NPs. The NiO—NPs electrode material delivered an excellent half-cell specific capacitance of 644 (~89.4 $mAhg^{-1}$) Fg^{-1} at 0.5 Ag^{-1}. The NiO—NPs|AC ASC device delivered maximum capacitance of ~280 Fg^{-1} (~38.8 $mAhg^{-1}$) and energy density of ~25 $Whkg^{-1}$ at ~40.1 Wkg^{-1} power density with 96.5% capacitance retention even after 10,000 cycles. Hence, this bio-synthesized NiO—NPs with high electrochemical stability can be a potential electrode material for energy and catalytic applications.

CRediT authorship contribution statement

Sivagaami Sundari Gunasekaran: Conceptualization, Methodology, Data curtion, Writing – original draft, Writing – review & editing. **Arthi Gopalakrishnan:** Conceptualization, Methodology, Data curtion, Writing – original draft, Writing – review & editing. **Raghu Subashchandrabose:** Conceptualization, Methodology, Data curtion, Writing – original draft, Writing – review & editing. **Sushmee Badhulika:** Funding acquisition, Investigation, Project administration, Resources, Supervision, Writing – review & editing.

Declaration of Competing Interest

There are no conflicts to declare.

Acknowledgment

SB acknowledges financial assistance from Scientific and Engineering Research Board (SERB) grant SB/WEA-03/2017.

References

[1] R. Dubey, V. Guruviah, Review of carbon-based electrode materials for supercapacitor energy storage, Ionics (Kiel) 25 (4) (2019) 1419–1445.
[2] C.V.M. Gopi, R. Vinodh, S. Sambasivam, I.M. Obaidat, H.J Kim, Recent progress of advanced energy storage materials for flexible and wearable supercapacitor: from design and development to applications, J. Energy Storage 27 (2020), 101035.
[3] C.V.M. Gopi, S. Sambasivam, K.V.G. Raghavendra, R. Vinodh, I.M. Obaidat, H. J Kim, Facile synthesis of hierarchical flower-like NiMoO4-CoMoO4 nanosheet arrays on nickel foam as an efficient electrode for high rate hybrid supercapacitors, J. Energy Storage 30 (2020), 101550.
[4] A.K. Das, N.H. Kim, S.H. Lee, Y. Sohn, J.H. Lee, Facile synthesis of porous CuCo2O4 composite sheets and their supercapacitive performance, Compos. Part B: Eng. 150 (2018) 234–241.
[5] S.H. Kim, R. Vinodh, C.V.M. Gopi, V.G.R. Kummara, S. Sambasivam, I.M. Obaidat, H.J Kim, Novel porous carbon material derived from hypercross-linked polymer of p-xylene for supercapacitors electrode, Mater. Lett. 263 (2020), 127222.
[6] T. Anitha, A.E. Reddy, R. Vinodh, H.J. Kim, Y.R. Cho, Preparation and characterization of CoWO4/CoMn2O4 nanoflakes composites on Ni foam for electrochemical supercapacitor applications, J. Energy Storage 30 (2020), 101483.
[7] R. Vinodh, C.V.M. Gopi, V.G.R. Kummara, R. Atchudan, T. Ahamad, S. Sambasivam, ..., H.J Kim, A review on porous carbon electrode material derived from hypercross-linked polymers for supercapacitor applications, J. Energy Storage 32 (2020), 101831.
[8] A.K. Das, S. Sahoo, P. Arunachalam, S. Zhang, J.J. Shim, Facile synthesis of Fe 3 O 4 nanorod decorated reduced graphene oxide (RGO) for supercapacitor application, RSC Adv. 6 (108) (2016) 107057–107064.
[9] A.K. Das, N.H. Kim, S.H. Lee, Y. Sohn, J.H. Lee, Facile synthesis of CuCo2O4 composite octahedrons for high performance supercapacitor application, Compos. Part B: Eng. 150 (2018) 269–276.
[10] A.D. Khalaji, M. Jarosova, P. Machek, K. Chen, D. Xue, Facile synthesis, characterization and electrochemical performance of nickel oxide nanoparticles prepared by thermal decomposition, Scr. Mater. 181 (2020) 53–57.
[11] W.C. Oh, K.N. Fatema, K.Y. Cho, M.R.U.D Biswas, Microwave-assisted synthesis of conducting polymer matrix based thin film NaLa (MoO4) 2-G-PPy composites for high-performance gas sensing, Surf. Interfaces 21 (2020), 100713.
[12] F. Mederos-Henry, S. Depaifve, A. Wolf, Y. Danlée, A. Delcorte, C. Bailly, S. Hermans, Nanocomposites with size-controlled nickel nanoparticles supported on multi-walled carbon nanotubes for efficient frequency-selective microwave absorption, Compos. Sci. Technol. 187 (2020), 107947.
[13] V. Londoño-Calderón, R. Ospina, J. Rodriguez-Pereira, S.A. Rincón-Ortiz, E. Restrepo-Parra, Molybdenum and nickel nanoparticles synthesis by laser ablation towards the preparation of a hydrodesulfurization catalyst, Catalysts 10 (9) (2020) 1076.
[14] A.C. Nwanya, M.M. Ndipingwi, C.O. Ikpo, R.M. Obodo, S.C. Nwanya, S. Botha, M. Maaza, Zea mays lea silk extract mediated synthesis of nickel oxide nanoparticles as positive electrode material for asymmetric supercabattery, J. Alloys Compd. 822 (2020), 153581.
[15] B.J. Reddy, P. Vickraman, A.S. Justin, Moringa oleifera leaf extract mediated reduced graphene oxide/α-Ni (OH) 2 nanocomposite for asymmetric supercapacitors, Brazil. J. Phys. 49 (3) (2019) 348–359.
[16] P. Alam, E. Ezzeldin, M. Iqbal, M.K. Anwer, G.A. Mostafa, M.H. Alqarni, F. Shakeel, Ecofriendly densitometric RP-HPTLC method for determination of rivaroxaban in nanoparticle formulations using green solvents, RSC Adv. 10 (4) (2020) 2133–2140.
[17] Z. Zhong, X. Gong, L. Wang, G. Bai, H. Wei, W. Yang, A facile way for fabrication of silver nanoparticle decorated graphene composites, Mater. Chem. Phys. 241 (2020), 122344.
[18] M.A. Peck, M.A. Langell, Comparison of nanoscaled and bulk NiO structural and environmental characteristics by XRD, XAFS, and XPS, Chem. Mater. 24 (23) (2012) 4483–4490.
[19] Y. Wu, Y. He, T. Wu, W. Weng, H. Wan, Effect of synthesis method on the physical and catalytic property of nanosized NiO, Mater. Lett. 61 (13) (2007) 2679–2682.
[20] N. Mironova-Ulmane, A. Kuzmin, I. Steins, J. Grabis, I. Sildos, M. Pärs, Raman scattering in nanosized nickel oxide NiO, J. Phys. Conf. Ser. 93 (December (1)) (2007), 012039.
[21] Y. Cheng, M. Guo, M. Zhai, Y. Yu, J. Hu, Nickel nanoparticles anchored onto Ni foam for supercapacitors with high specific capacitance, J. Nanosci. Nanotechnol. 20 (4) (2020) 2402–2407.
[22] C. Philippe, T. Suzuki, Z.-G. Zhang, T. Kyotani, A. Tomita, XPS of nitrogen-containing functional groups formed during the C– NO reaction, Energy Fuels 11 (3) (1997) 681–685.
[23] A.C. Sonavane, A.I. Inamdar, D.S. Dalavi, H.P. Deshmukh, P.S. Patil, Simple and rapid synthesis of NiO/PPy thin films with improved electrochromic performance, Electrochim. Acta 55 (7) (2010) 2344–2351.
[24] L. Hu, W. Chen, X. Xie, N. Liu, Y. Yang, H. Wu, Y. Cui, Symmetrical MnO2–carbon nanotube–textile nanostructures for wearable pseudocapacitors with high mass loading, ACS Nano 5 (11) (2011) 8904–8913.
[25] J.K. Chang, W.T. Tsai, Material characterization and electrochemical performance of hydrous manganese oxide electrodes for use in electrochemical pseudocapacitors, J. Electrochem. Soc. 150 (10) (2003) A1333.
[26] M. Liang, M. Zhao, H. Wang, J. Shen, X. Song, Enhanced cycling stability of hierarchical NiCo 2 S 4@ Ni (OH) 2@ PPy core–shell nanotube arrays for aqueous asymmetric supercapacitors, J. Mater. Chem. A 6 (6) (2018) 2482–2493.
[27] S. Xiong, S. Jiang, J. Wang, H. Lin, M. Lin, S. Weng, J. Chen, A high-performance hybrid supercapacitor with NiO derived NiO@ Ni-MOF composite electrodes, Electrochim. Acta (2020), 135956.
[28] K.V.G. Raghavendra, T.V.M. Sreekanth, T.J. Ko, J. Kim, K. Yoo, Facile hydrothermal synthesis of novel ZnWO4/ZnCo2O4 electrode for high-performance supercapacitors, Mater. Lett. (2021) 129296.
[29] Y. Zhang, Y. Shen, X. Xie, W. Du, L. Kang, Y. Wang, B. Wang, One-step synthesis of the reduced graphene oxide@ NiO composites for supercapacitor electrodes by electrode-assisted plasma electrolysis, Mater. Des. 196 (2020), 109111.
[30] S.D. Dhas, P.S. Maldar, M.D. Patil, A.B. Nagare, M.R. Waikar, R.G. Sonkawade, A. V. Moholkar, Synthesis of NiO nanoparticles for supercapacitor application as an efficient electrode material, Vacuum 181 (2020), 109646.

[31] Q. Yin, D. Li, J. Zhang, Y. Zhao, J. Luo, M. Shao, J. Han, An all-solid-state fiber-type supercapacitor based on hierarchical Ni/NiO@ CoNi-layered double hydroxide core-shell nanoarrays, J. Alloys Compd. 813 (2020), 152187.
[32] V.G.R. Kummara, V. Rajangam, V.M.G. Chandu, M.R. Kummara, H.J Kim, Facile synthesis of hierarchical agglomerated cauliflower-like ZnWO4@ NiO nanostructures as an efficient electrode material for high-performance supercapacitor applications, Mater. Lett. 268 (2020), 127594.
[33] H. Vijeth, S.P. Ashokkumar, L. Yesappa, M. Vandana, H. Devendrappa, Hybrid core-shell nanostructure made of chitosan incorporated polypyrrole nanotubes decorated with NiO for all-solid-state symmetric supercapacitor application, Electrochim. Acta 354 (2020), 136651.
[34] N. Jayababu, S. Jo, Y. Kim, D. Kim, Preparation of NiO decorated CNT/ZnO core-shell hybrid nanocomposites with the aid of ultrasonication for enhancing the performance of hybrid supercapacitors, Ultrason. Sonochem. 71 (2020), 105374.
[35] M. Kang, H. Zhou, B. Qin, N. Zhao, B. Lv, Ultrathin nanosheet-assembled, phosphate ion-functionalized NiO microspheres as efficient supercapacitor materials, ACS Appl. Energy Mater. 3 (10) (2020) 9980–9988.
[36] F. Cao, G.X. Pan, X.H. Xia, P.S. Tang, H.F. Chen, Synthesis of hierarchical porous NiO nanotube arrays for supercapacitor application, J. Power Sources 264 (2014) 161–167.
[37] Z. Yang, F. Xu, W. Zhang, Z. Mei, B. Pei, X. Zhu, Controllable preparation of multishelled NiO hollow nanospheres via layer-by-layer self-assembly for supercapacitor application, Period. Power Sources 246 (2014) 24–31.
[38] D. Han, X. Jing, J. Wang, P. Yang, D. Song, J. Liu, Porous lanthanum doped NiO microspheres for supercapacitor application, J. Electroanal. Chem. 682 (2012) 37–44.
[39] B. Ren, M. Fan, Q. Liu, J. Wang, D. Song, X. Bai, Hollow NiO nanofibers modified by citric acid and the performances as supercapacitor electrode, Electrochim. Acta 92 (2013) 197–204.
[40] I. Shaheen, K.S. Ahmad, C. Zequine, R.K. Gupta, A.G. Thomas, M.A. Malik, Effect of NiO on organic framework functionalized ZnO nanoparticles for energy storage application, Int. J. Energy Res. 44 (7) (2020) 5259–5271.
[41] H. Shi, M. Ma, P. Liu, X. Jia, F. Yang, B. Zhao, Z. Li, Preparation of petal-particle cross-linking flowerlike NiO for supercapacitor application, J. Electroanal. Chem. 876 (2020), 114481.
[42] S. Vijayakumar, S. Nagamuthu, G. Muralidharan, Supercapacitor studies on NiO nanoflakes synthesized through a microwave route, ACS Appl. Mater. Interfaces 5 (6) (2013) 2188–2196.
[43] X. Zhang, W. Shi, J. Zhu, W. Zhao, J. Ma, S. Mhaisalkar, Q. Yan, Synthesis of porous NiO nanocrystals with controllable surface area and their application as supercapacitor electrodes, Nano. Res. 3 (9) (2010) 643–652.
[44] U.M. Patil, R.R. Salunkhe, K.V. Gurav, C.D. Lokhande, Chemically deposited nanocrystalline NiO thin films for supercapacitor application, Appl. Surf. Sci. 255 (5) (2008) 2603–2607.
[45] H. Xiao, S. Yao, H. Liu, F. Qu, X. Zhang, X. Wu, NiO nanosheet assembles for supercapacitor electrode materials, Prog. Natl. Sci.: Mater.Int. 26 (3) (2016) 271–275.
[46] J. Zhu, J. Jiang, J. Liu, R. Ding, H. Ding, Y. Feng, X. Huang, Direct synthesis of porous NiO nanowall arrays on conductive substrates for supercapacitor application, J. Solid State Chem. 184 (3) (2011) 578–583.
[47] G.S. Gund, C.D. Lokhande, H.S. Park, Controlled synthesis of hierarchical nanoflake structure of NiO thin film for supercapacitor application, J. Alloys Compd. 741 (2018) 549–556.